

Lawrence Berkeley National Laboratory

Recent Work

Title

A SILICON-29 NUCLEAR MAGNETIC RESONANCE STUDY OF SILICON-ALUMINUM ORDERING IN LEUCITE AND ANALCITE

Permalink

<https://escholarship.org/uc/item/38t1j4n8>

Author

Murdoch, J.B.

Publication Date

1986-07-01



Lawrence Berkeley Laboratory

UNIVERSITY OF CALIFORNIA

RECEIVED
LAWRENCE
BERKELEY LABORATORY

Materials & Molecular Research Division

JAN 22 1987

LIBRARY AND
DOCUMENTS SECTION

Submitted to Physics and Chemistry of Minerals

A SILICON-29 NUCLEAR MAGNETIC RESONANCE STUDY
OF SILICON-ALUMINUM ORDERING IN LEUCITE AND
ANALCITE

J. B. Murdoch, J.F. Stebbins, I.S.E. Carmichael,
and A. Pines

July 1986

TWO-WEEK-LOAN COPY

*This is a Library Circulating Copy
which may be borrowed for two weeks.*



LBL-22552
^{c.2}

DISCLAIMER

This document was prepared as an account of work sponsored by the United States Government. While this document is believed to contain correct information, neither the United States Government nor any agency thereof, nor the Regents of the University of California, nor any of their employees, makes any warranty, express or implied, or assumes any legal responsibility for the accuracy, completeness, or usefulness of any information, apparatus, product, or process disclosed, or represents that its use would not infringe privately owned rights. Reference herein to any specific commercial product, process, or service by its trade name, trademark, manufacturer, or otherwise, does not necessarily constitute or imply its endorsement, recommendation, or favoring by the United States Government or any agency thereof, or the Regents of the University of California. The views and opinions of authors expressed herein do not necessarily state or reflect those of the United States Government or any agency thereof or the Regents of the University of California.

A Silicon-29 Nuclear Magnetic Resonance Study of Silicon-Aluminum
Ordering in Leucite and Analcite

J.B. Murdoch,* J.F. Stebbins,[†] I.S.E. Carmichael, and A. Pines

Lawrence Berkeley Laboratory
University of California
Berkeley, California 94720

*Technicare Corporation, Cleveland, OH 44101; Present Address: Picker
International, Inc., Highland Heights, OH 44143

[†]Stanford University, Stanford, CA 94305

ABSTRACT

Silicon-29 magic-angle-spinning NMR spectroscopy has been used to investigate the silicon-aluminum distribution in natural samples of analcite and leucite (before and after heat treatment) as well as a leucite synthesized from a gel. Two different simulation programs were developed to fit the experimental spectra. The first is based on three assumptions: a different aluminum occupancy fraction g_i for each of the three crystallographically distinct tetrahedral sites T_i in leucite, the existence of Loewenstein's aluminum-avoidance effect, and an otherwise random arrangement of tetrahedral cations. The second interchanges Al and Si cations on a lattice of $3 \times 3 \times 3$ unit cells to generate an optimized fit within the constraint of aluminum avoidance. Both models predict that the T_2 sites in natural leucite are deficient in aluminum; model 2 yields $g_1=0.37$, $g_2=0.14$, and $g_3=0.48$ for the fractional Al occupancy at each site. Heat treatment at 1673K for a week has no apparent effect on these values. Aluminum occupancies in the gel-synthesized leucite are somewhat more uniform: $g_1=0.36$, $g_2=0.18$, and $g_3=0.42$.

In simulating the spectrum of analcite, two distinctly different Si-Al distributions are obtained: (A) $g_1=g_3=0.09$, $g_2=0.78$ and (B) $g_1=g_3=0.46$, $g_2=0.04$. Additional NMR measurements on an ion-exchanged sample or an accurate determination of unit-cell dimensions could resolve this ambiguity.

INTRODUCTION

In a previous paper (Stebbins et al. 1986), we described the use of silicon-29 nuclear magnetic resonance (NMR) spectroscopy to study defects and short-range order in nepheline group minerals. Here we apply the same technique to investigate the distribution of silicon and aluminum atoms in a second class of feldspathoid minerals, developing in the process two general computational methods to find distributions that best match experimental spectra. Phase transitions in most of the samples we will discuss have also been examined recently using differential scanning calorimetry (Lange et al. 1986).

Leucite (KAlSi_2O_6) and analcite ($\text{NaAlSi}_2\text{O}_6 \cdot \text{H}_2\text{O}$) are silica-poor alkali aluminosilicates with the same topographical arrangement of tetrahedral cations. As in feldspars, zeolites, and the silica polymorphs, the tetrahedra -- SiO_4 or AlO_4 -- form a three-dimensional network structure, with every tetrahedron connected to four others. X-ray and neutron diffraction measurements on single crystals of these minerals (e.g. Taylor 1930; Peacor 1968; Ferraris et al. 1972; Mazzi et al. 1976; Mazzi and Galli 1978) can be used to determine the average coordinates of the tetrahedral sites in the unit cell. However, because diffraction techniques inherently measure long-range averages, determining the true local distribution of silicon and aluminum atoms among these sites is often not possible. In particular, short-range disorder often cannot be distinguished from long-range disorder that results from domain structure. In contrast, NMR provides a direct, complementary look at short-range structure: a nucleus with non-zero spin is used as a probe of its local electronic environment. The chemical shielding (or chemical shift) characterizes the extent to

which nearby electrons shield the nucleus from a large static magnetic field. Nuclei in different sites are shielded differently and as a result absorb energy at different frequencies.

However, the orientational anisotropy of chemical shielding gives rise to broadening in the NMR spectrum of a polycrystalline solid. In favorable cases, the distinctive powder pattern lineshape that results for each type of site can be analyzed to yield the three principal values of its chemical shielding tensor. Alternatively, when broadening obscures the differentiation of sites, it can be removed by rapidly spinning the sample about an axis inclined at the "magic" angle, 54.7° , relative to the external magnetic field (Andrew 1981). Each powder pattern lineshape gives rise to a center peak at the isotropic chemical shift value, flanked by a series of spinning sideband peaks spaced at the sample rotation frequency. When the rotation rate is high enough, the sidebands disappear: for each distinct chemical environment, one obtains a sharp line corresponding to the isotropic chemical shift value, much as one sees in the NMR spectra of liquids.

As pioneered by Lippmaa et al. (1980,1981), silicon-29 magic-angle-spinning (MAS) NMR has been of particular use in the study of silicate structure. Spectra are better resolved than those of most other "NMR-active" nuclei of relevance in mineralogy, such as ^{27}Al , ^{23}Na , ^{11}B , or ^{17}O , because unlike these species, the spherical silicon-29 nucleus experiences no nuclear quadrupole coupling to local electric field gradients. Moreover, the value of the isotropic chemical shift δ (measured in ppm relative to a tetramethylsilane standard) sensitively and systematically reflects the bonding environment of a silicon nucleus. The value of δ becomes more negative (reflecting greater shielding of the Si nucleus) as

the degree of silicate polymerization increases, from monomeric SiO_4^{4-} units to a three-dimensional network of tetrahedra, changing by roughly -10 ppm for each additional bridging oxygen. The identity of the adjacent tetrahedral cations also affects the chemical shift: for each increase in the number of aluminum neighbors, a silicon is deshielded (δ less negative) by approximately 6 ppm. This relationship has been of major importance in the elucidation of silicon-aluminum ordering in zeolites (e.g. Lippmaa et al. 1981; Fyfe et al. 1983). The silicon chemical shift has in addition been correlated with a number of interrelated structural features, including the average Si-O-T bond angle (Smith and Blackwell 1983; Thomas et al. 1983; Ramdas and Klinowski 1984), the sum of the cation-oxygen bond strengths surrounding a silicon (Smith et al. 1983), the average Si-O bond length (Higgins and Woessner 1982; Grimmer and Radeaglia 1984), and the estimated s-character of oxygen or Si-O orbitals (Engelhardt and Radeaglia 1984; Radeaglia and Engelhardt 1985; Grimmer 1985).

Aluminum-27 MAS NMR could also be used to study silicon-aluminum ordering in leucite minerals, although spectral resolution would likely be degraded by second-order nuclear quadrupole coupling. Because all of our magic-angle-spinning probe rotors and stators were at the time constructed of alumina, we did not attempt these measurements.

SAMPLE CHARACTERIZATION

We have examined three samples of natural leucite (one before and after heat treatment), one natural analcite specimen, and a synthetic leucite. Compositional data for the leucite samples, mostly based on electron microprobe measurements, have been presented by Lange et al.

(1986). The associated silicon-to-aluminum ratios are listed in Table 1. Powder diffraction data on all samples confirmed that they were pure, and for the synthetic phase, that the desired product was obtained.

Two samples were obtained from leucite-rich volcanic rocks in the Roman District, Italy: the first (labeled "89-21" in Lange et al. 1986) from Mt. Cimini, the second (University of California, Berkeley, Department of Geology and Geophysics, collection number 16682; labeled "90-05" by Lange et al.) from Rocca Monfina. Each is close in composition to the ideal stoichiometry KAlSi_2O_6 . The two samples yielded very nearly identical ^{29}Si MAS NMR spectra, which we therefore averaged together to improve the overall signal-to-noise ratio. (The combination will be referred to as "natural leucite.") In addition, to study thermal effects on Si-Al ordering, a portion of the Mt. Cimini sample was heat treated at 1673K for one week.

The third leucite sample (labeled "1774" in Lange et al. 1986), which exhibits no optically observable twinning, is from the groundmass of a wyomingite lava obtained, appropriately enough, in the Leucite Hills of Wyoming (Carmichael 1967). It contains 2.3 wt. % Fe and has a higher Si/Al ratio (2.35) than the other feldspathoid samples we have examined.

To investigate the effect of excess SiO_2 in solid solution, a synthetic leucite was prepared as a gel, then dehydrated and heated in a Pt crucible for 3 days at 1373K, followed by 5 days at 1773K (Lange et al. 1986, sample SL.2). Electron microprobe and wet chemical data indicate that the product is approximately 86 wt. % KAlSi_2O_6 and 14 wt. % KAlSi_3O_8 .

The analcite sample was in the form of colorless needles from Golden, Colorado (composition by weight from electron microprobe data: 56.8% SiO_2 , 22.7% Al_2O_3 , and 14.1% Na_2O , with 8.0% H_2O specified). A portion of this

sample was dehydrated for 23 hours at 1033K. In turn, part of the dehydrated sample was used to create a potassium-exchanged analcite by heating it in molten KBr at 1033K for 44 hours. This procedure is not expected to affect the distribution of Al and Si cations (Waldbaum and Robie 1971). Intriguingly, however, the resulting leucite gave no ^{29}Si NMR signal. The likely reason for this lack of response will be discussed later.

EXPERIMENTAL DETAILS

As in previous work (Stebbins et al. 1986), spectra were obtained on a "home-built" Fourier transform NMR spectrometer operating at 8.5 tesla with a magic-angle-spinning probe from Doty Scientific. Powdered samples were spun in alumina rotors at 2.5-3.5 kHz, and spinning sideband peaks were small for all samples except the wyomingite leucite.

From 660 to 8300 free induction decays were acquired and averaged together for each spectrum. The rf pulse tip angle was approximately 45° , and successive pulses were spaced at 4-120 seconds to avoid spectral distortion resulting from incomplete spin-lattice (T_1) relaxation. Silicon chemical shifts were measured relative to an external sample of tetramethylsilane or relative to a secondary standard: a spinning sample of crystalline jadeite ($\text{NaAlSi}_2\text{O}_6$, $\delta = -92.0$ ppm). Except for the case of analcite and wyomingite leucite, no apodization of free induction decay signal was performed prior to Fourier transformation. Apodization of these data gave rise to an increase in linewidth of at most a few percent.

Spectra were analyzed and deconvoluted using a modification of a peak-fitting program originally developed for Raman spectra (Mysen et al. 1982).

Individual peaks were assumed to be Gaussian, mirroring the statistically normal distribution of bond length and bond angle values expected in a disordered crystal. We limited the number of components in the lineshape-fitting process to the number of readily apparent peaks or shoulders in the spectrum, then let the program freely vary the position, height, and width of each component to obtain an optimal fit. The output includes an estimated standard deviation for each peak area; these values were incorporated in subsequent structural analysis.

For all analyzed spectra, the small spinning sideband lineshapes were not included in the deconvolution process: their lower signal-to-noise ratio plus some roll in the baseline made a quantitative multi-component fit problematic. Omission of the sidebands introduces some error in the relative peak areas for each silicon type, which in turn affects the structural interpretation. However, we believe that this source of error can be neglected relative to the uncertainties in deconvolution of the center peaks. Except in the case of the wyomingite leucite (which was only examined qualitatively), no sideband was more than roughly 15% as high as the corresponding center peak. Moreover, the sideband lineshapes, when distinguishable, were miniature versions of the center peaks, suggesting that, as one might expect, chemical shift anisotropies associated with the different silicon sites do not vary widely. Hence center peak areas are probably scaled down uniformly relative to total peak areas.

STRUCTURAL CONSIDERATIONS

Before discussing the NMR spectra we have obtained, a closer look at the connectivity of tetrahedral cations in leucite minerals is necessary.

There are 48 tetrahedral sites in the unit cell, which is cubic (or nearly so) for analcite and pollucite [a naturally occurring cesium analog, general formula $\text{Cs}_x\text{Na}_y\text{Al}_{x+y}\text{Si}_{48-x-y}\text{O}_{96}\cdot(16-x)\text{H}_2\text{O}$ (Beger 1969)] and tetragonal for leucite itself. Galli et al. (1978) have presented an elegant model for visualizing the intricate tetrahedral framework. As noted also by Merlino (1984), the building block for this idealized structure can be considered to be a square prism with two of the long edges missing. The structure of a unit cell is shown in Fig. 1, a view looking approximately along the c -axis. The circles represent tetrahedral cations (Al or Si), and intervening oxygens are omitted. Three sets of the aforementioned prisms can be seen, each set oriented parallel to one of the unit cell axes. The three sets of crystallographically distinct tetrahedral sites T_i for low temperature leucite ($I4_1/a$ symmetry) are also apparent. Each tetrahedral node is part of two four-membered rings (end pieces of the prisms) and two six-membered rings (which appear chair-shaped in this representation). Not shown are the two types of interstitial sites occupied by charge-balancing alkali cations or water molecules: the so-called S sites, located at the center of each prism, and the W sites, located midway along the missing edges of each prism. There are 24 S sites and 16 W sites per unit cell (Galli et al. 1978).

The topologic symmetry (Smith 1982) of the unit cell in Fig. 1 is cubic: $Ia3d$, with all tetrahedral sites equivalent. Assuming a random arrangement of tetrahedral cations Al and Si, the topochemical symmetry (a long-range average over a multitude of unit cells) is also $Ia3d$. However, variation in the size of the extra-framework species present can induce structural distortion and lower the real symmetry. In pollucite, large Cs^+ ions (and water molecules in some samples) occupy the W sites, and the

overall cubic symmetry is maintained. In analcite, $\text{NaAlSi}_2\text{O}_6 \cdot \text{H}_2\text{O}$, water molecules occupy the W sites and sodium ions occupy two-thirds of the S sites (Galli et al. 1978). Its structure has also been characterized as cubic (Taylor 1930; Ferraris et al. 1972), but more recent work (Mazzi and Galli 1978) indicates that small deviations can exist and that the real symmetry is lower. Some samples were found by these authors to be tetragonal: $I4_1/acd$, with sites T_1 and T_3 in Fig. 1 equivalent and either $c > a$ or $a > c$. Others were found to be orthorhombic ($Iabc$).

In leucite, potassium ions occupy the W sites and the S sites are vacant. Above roughly 900K, the symmetry is $Ia3d$ as in pollucite (Peacor 1968). At lower temperatures, however, because K^+ is smaller than either Cs^+ or H_2O , the framework structure collapses around the potassium ions to maintain a favorable K-O distance. The tetragonal symmetry that results is $I4_1/a$, with $a = 13.09 \text{ \AA}$, $c = 13.75 \text{ \AA}$ (Mazzi et al. 1976). The characteristic four-fold screw axes parallel to the c -axis are apparent in Fig. 1.

Inversion from the high-temperature cubic phase to the low-temperature tetragonal phase also gives rise to extensive merohedric and pseudomerohedric twinning (Mazzi et al. 1976). However, because MAS NMR is a probe of short-range structure, the presence of twinning will have an effect on the leucite ^{29}Si spectrum only if silicons on the twin boundaries are a measurable fraction (at least one percent) of the total number of silicons present and if these silicons have a different chemical shift as a result of site distortion.

One may note that there are three varieties of four-membered rings in the leucite structure: one with four T_1 sites, one with four T_3 sites, and one composed of two T_2 sites, a T_1 site, and a T_3 site. The sites themselves can be further distinguished as follows:

Each T_1 site has two T_1 neighbors and two T_2 neighbors.

Each T_2 site has two T_1 neighbors and two T_3 neighbors.

Each T_3 site has two T_2 neighbors and two T_3 neighbors.

Because the chemical shift of a silicon-29 nucleus depends on the identity -- Si or Al -- of adjacent tetrahedral cations, such connectivity information is crucial for interpreting the NMR lineshape and determining the nature of Si-Al ordering.

With this background, we can now examine how silicon and aluminum are distributed on the lattice of tetrahedral sites. Single-crystal x-ray diffraction results suggest that the arrangement is completely random in leucite and pollucite, and random in analcite but with enrichment of Al in one type of site and Si in the other (Galli et al. 1978).

NMR data provide information directly on local cation distributions. In particular, previous work on a wide variety of aluminosilicates, including other feldspathoid minerals (Stebbins et al. 1986), has demonstrated that one constraint on tetrahedral cation disorder is of general validity: the aluminum-avoidance principle or "Loewenstein's rule" (Loewenstein 1954), which states that energetically unfavorable Al-O-Al linkages do not occur in aluminosilicates for which the Si/Al ratio is greater than or equal to one. Occasional exceptions exist, such as crystalline cordierite prepared with minimal annealing (Putnis et al. 1985), but we will assume the existence of an aluminum-avoidance effect in our analysis of leucite and analcite. (As will be shown, our data are indeed consistent with this assumption.)

RESULTS

Analcite

Fig. 2 displays the ^{29}Si MAS NMR spectrum of analcite; results of the peak-fitting program are listed in Table 2. Because the tetrahedral sites $T_1=T_3$ and T_2 are very nearly equivalent, ^{29}Si chemical shifts are a function only of the number of aluminum neighbors -- there is no "intrinsic" shift difference between sites. Hence each peak in Fig. 2 corresponds to silicons on all T_1 sites with a fixed number of $-O-Al$ linkages.

Peak assignments can be made using one of several empirical formulas that relate $\underline{\delta}_{\text{Si}}$ to particular structural parameters. For example, Ramdas and Klinowski (1984) have found that $\underline{\delta}_{\text{Si}}$ in tectosilicates can be expressed as the sum of a constant term, a term proportional to the average distance to adjacent tetrahedral cations (expressed in terms of $\underline{\theta}$, the average Si-O-T bond angle), and an electrostatic deshielding term proportional to \underline{k} , the number of Al neighbors. Combining their Eqs. 1 and 2 yields the following relationship:

$$\underline{\delta} = 143.03 - (263.61 + 2.64\underline{k}) \sin \underline{\theta}/2 + 7.95\underline{k} \quad (1)$$

Using bond angles obtained by Mazzi and Galli (1978) for several different analcite samples, one finds $\underline{\theta}(T_1)=\underline{\theta}(T_2)=144.5^\circ$ and $\underline{\delta}(0Al)=-108.0$ ppm, $\underline{\delta}(1Al)=-102.5$ ppm, $\underline{\delta}(2Al)=-97.1$ ppm, $\underline{\delta}(3Al)=-91.7$ ppm, and $\underline{\delta}(4Al)=-86.2$ ppm. These estimated chemical shifts are in good agreement with experimental values and substantiate the peak assignments in Fig. 2 and Table 2. Note that there are apparently no silicons present with four Al

neighbors. The silicon-to-aluminum ratio \underline{R} can be obtained from the relative peak areas \underline{I}_k . The average number of aluminum neighbors per silicon is given by

$$\langle k \rangle = \sum k \underline{I}_k / \sum \underline{I}_k \quad ; \quad (2)$$

if Loewenstein's rule is obeyed,

$$\underline{R} = 4 / \langle k \rangle \quad (3)$$

(Klinowski et al. 1982). Using the peak areas for analcite, one finds $\langle k \rangle = 1.87$ and $\underline{R} = 2.14$, in excellent agreement with the electron microprobe measurement listed in Table 1. Were a substantial number of Al-O-Al linkages present, the value of \underline{R} obtained using Eq. 3 would be considerably larger than the microprobe result. We will return to the analysis of analcite peak areas in a later section.

The ^{29}Si MAS NMR spectrum of an analcite sample dehydrated at 1033K for 23 hours is displayed in Fig. 3. The absence of water molecules in the W sites has apparently distorted the tetrahedral framework, broadening the peaks associated with each type of silicon present and increasing the overall range of chemical shifts. Because the spectrum lacks distinct "bumps" and shoulders, however, we have not attempted to deconvolute it into a sum of Gaussian components.

As stated earlier, we also prepared a potassium-exchanged dehydrated analcite that unfortunately gave rise to no measurable ^{29}Si NMR signal. We believe that this lack of response is a consequence of an extremely long ^{29}Si spin-lattice relaxation time \underline{T}_1 . [\underline{T}_1 is the characteristic time for

nuclear spin state populations to return to their equilibrium values (following rf pulse perturbation) via energy exchange with their surroundings.] Indeed, there is a likely reason why T_1 (not to be confused with the tetrahedral site designation) should be longer in our potassium-exchanged analcite than in the untreated original sample. In non-porous silicates, the predominant coupling pathway between nuclear spin states and the lattice is via the unpaired electrons in paramagnetic impurities, e.g. Fe^{2+} or Fe^{3+} ions (Barron et al. 1983). [Nuclei near the paramagnetic species relax rapidly; adjacent nuclei in an expanding shell are then relaxed by a process known as spin diffusion: an energy-conserving "flip-flop" of nuclear states (Abragam 1961).] The concentration of paramagnetic ions, low to begin with in our microprobe standard analcite specimen, was no doubt further reduced in the high-temperature ion exchange process. The resulting impurity concentration was apparently less than in our gel-synthesized leucite sample, for which a spectrum was readily obtained.

Leucite

The averaged ^{29}Si MAS NMR spectrum obtained for the Mt. Cimini and Rocca Monfina leucite samples is displayed in Fig. 4. The lineshape was not appreciably altered by varying the delay between successive rf pulses from 5 to 40 seconds, suggesting that all the silicons present have roughly the same spin-lattice relaxation time. The spectrum of the heat-treated Mt. Cimini leucite sample appears in Fig. 5 and that of the gel-synthesized leucite in Fig. 6. Each of the three lineshapes was deconvoluted into the sum of eight Gaussian components, as detailed in Table 3.

Peak assignments and the analysis of intensities will be discussed in the next section. We note here, however, that heat treatment of leucite at

1673K for a week has at most a minimal effect on its ^{29}Si NMR spectrum and hence on the nature of its short-range Si-Al order. As observed by differential scanning calorimetry, heat treatment did lower the tetragonal-cubic phase transition temperature by 24° and better resolved two peaks on the heat capacity curve (Lange et al. 1986). We should also note that prior to quantitatively deconvoluting the leucite spectrum on the computer, we incorrectly described it in a preliminary report as a series of sharp peaks centered on a broad background absorption (Murdoch et al. 1984).

The wyomingite leucite spectrum is shown in Fig. 7. Because of the low signal-to-noise ratio, no peak fitting was attempted, but it is apparent that a different Si-Al distribution must exist in this sample than in the other leucites. In addition, as mentioned earlier, spinning sidebands for this sample are noticeably larger. This sideband enhancement is the result of an anisotropic coupling to the unpaired electrons associated with the 2.3 wt. % iron present. The same effect has been seen in glasses prepared from silicic lavas (Murdoch et al. 1985).

INTERPRETATION OF THE LEUCITE SPECTRA

Our goal is to use relative peak areas from the deconvolution program to determine the distribution of silicon and aluminum cations among the different T_i sites. Similar analyses have been published recently for cordierite (Putnis et al. 1985; Putnis and Angel 1985) and synthetic mazzite (Jarman et al. 1984; Klinowski and Anderson 1986).

The first step is peak assignment. There are three inequivalent tetrahedral sites in low-temperature leucite, and for each a silicon can have 0 to 4 aluminum neighbors. Hence there can exist 15 distinct silicon

species; these must be matched with the eight experimental peaks. To this end, we turn again to the linear relationship between δ_{Si} and the average Si-O-T bond angle derived empirically by Ramdas and Klinowski (1984).

Using the bond angles obtained from single-crystal x-ray diffraction data by Mazzi et al. (1976), we can estimate the chemical shift for each of the 15 silicon species, as listed in Table 4. Note that the estimated intrinsic shift between $T_1(OAl)$ and $T_3(OAl)$ silicons is 12.7 ppm, a larger intrinsic shift than has been seen in zeolites. Note also that the average Si-O-T bond angle for site T_1 is nearly the same as that for all tetrahedra in analcite. We expect, therefore, that T_1 silicons contribute to the four leucite peaks (5-8) that coincide with peaks in the analcite spectrum.

A more detailed comparison of the estimated chemical shifts with the experimental values in Table 3 suggests that assignment scheme I in table 5 is the correct way to match $T_{\underline{i}}(kAl)$ silicons with peaks in the spectrum. (To an extent, relative peak widths are also in accord with this model: peaks 1 and 2, each corresponding to one type of silicon, are narrower than peaks 5-7, each of which corresponds to at least two Si species whose chemical shifts may not exactly overlap. However, peaks 3 and 4 are narrower than one might expect and peak 8 is broader.) Other assignment schemes, labeled II, III, and IV in Table 5, cannot immediately be ruled out; however, we shall find that scheme I provides the best fit to experimental peak areas and the experimental Si/Al ratio.

Two different approaches have been taken in modeling leucite and its NMR spectra on the computer. The first assumes a different aluminum occupancy value for each of the three $T_{\underline{i}}$ sites and the existence of an aluminum-avoidance effect, but an otherwise random distribution of Al and Si. The second begins with some initial distribution of Al and Si on a

3×3×3-unit-cell lattice of sites, then generates random Al jumps (subject to aluminum avoidance) to obtain a progressively better fit to the eight experimental peak areas.

Model 1

Assume we have \underline{N} T_1 sites, \underline{N} T_2 sites, and \underline{N} T_3 sites with the connectivity of the leucite lattice, where \underline{N} is the proverbial large number. These give rise to \underline{N} T_1 - T_1 bonds (omitting the intervening oxygens), \underline{N} T_3 - T_3 bonds, $2\underline{N}$ T_1 - T_2 bonds, and $2\underline{N}$ T_2 - T_3 bonds, but no T_1 - T_3 or T_2 - T_2 bonds. Let \underline{g}_1 , \underline{g}_2 , and \underline{g}_3 be the fraction of each type of site occupied by aluminum. If we define

$$\langle \underline{g} \rangle = (\underline{g}_1 + \underline{g}_2 + \underline{g}_3) / 3 \quad , \quad (4)$$

then the Si/Al ratio is given by

$$\underline{R} = \frac{1 - \langle \underline{g} \rangle}{\langle \underline{g} \rangle} \quad . \quad (5)$$

Keeping in mind the aluminum-avoidance rule, we can list the total number of Si-Al bonds:

$$\begin{aligned} & 2\underline{N}\underline{g}_1 \text{ Si}[T_1] \text{ to Al}[T_1] \text{ bonds} \ , \\ & 2\underline{N}\underline{g}_1 \text{ Si}[T_2] \text{ to Al}[T_1] \text{ bonds} \ , \\ & 2\underline{N}\underline{g}_2 \text{ Si}[T_1] \text{ to Al}[T_2] \text{ bonds} \ , \\ & 2\underline{N}\underline{g}_2 \text{ Si}[T_3] \text{ to Al}[T_2] \text{ bonds} \ , \\ & 2\underline{N}\underline{g}_3 \text{ Si}[T_2] \text{ to Al}[T_3] \text{ bonds} \ , \\ & 2\underline{N}\underline{g}_3 \text{ Si}[T_3] \text{ to Al}[T_3] \text{ bonds} \ . \end{aligned}$$

The probability of each is found by dividing the number of bonds from Si[T_i] to Al[T_j] by the total number of bonds from Si[T_i] to a T_j site:

$$\underline{P}(\underline{i}, \underline{j}) = \frac{2\underline{N}g_{\underline{i}}}{2\underline{N}(1 - g_{\underline{i}})} = \frac{g_{\underline{i}}}{1 - g_{\underline{i}}} \quad (6)$$

In turn, the probability of a Si[$T_{\underline{i}}$] to Si[$T_{\underline{j}}$] bond is given by

$$\underline{Q}(\underline{i}, \underline{j}) = 1 - \underline{P}(\underline{i}, \underline{j}) = \frac{1 - g_{\underline{i}} - g_{\underline{j}}}{1 - g_{\underline{i}}} \quad (7)$$

Note that to keep probabilities greater than or equal to zero and less than or equal to one, we must have

$$g_1 \leq 0.5 \quad , \quad (8a)$$

$$g_3 \leq 0.5 \quad , \quad (8b)$$

$$g_2 \leq 1 - g_1 \quad , \quad (8c)$$

$$g_2 \leq 1 - g_3 \quad . \quad (8d)$$

These constraints are a consequence of Loewenstein's rule.

To further compress notation, we now relabel the following single-bond aluminum-neighbor probabilities: $\underline{a}_1 = \underline{P}(1,1)$, $\underline{b}_1 = \underline{P}(1,2)$, $\underline{a}_2 = \underline{P}(2,1)$, $\underline{b}_2 = \underline{P}(2,3)$, $\underline{a}_3 = \underline{P}(3,2)$, and $\underline{b}_3 = \underline{P}(3,3)$. In addition, we define analogous Si-neighbor probabilities: $\underline{c}_{\underline{i}} = 1 - \underline{a}_{\underline{i}}$ and $\underline{d}_{\underline{i}} = 1 - \underline{b}_{\underline{i}}$. To obtain an expression for $\underline{n}_{\underline{i}}(\underline{k})$, the number of silicons in site $T_{\underline{i}}$ with \underline{k} adjacent Al cations, we must multiply the population of silicons in site $T_{\underline{i}}$, $\underline{N}(1 - g_{\underline{i}})$, by the probability of their having \underline{k} Al neighbors. This probability is given by the sum of the probabilities for different Al arrangements:

$$\underline{n}_i(4) = \underline{N}(1-\underline{g}_i)(\underline{a}_i^2 \underline{b}_i^2), \quad (9a)$$

$$\underline{n}_i(3) = \underline{N}(1-\underline{g}_i)(2\underline{a}_i \underline{c}_i \underline{b}_i^2 + 2\underline{a}_i^2 \underline{b}_i \underline{d}_i), \quad (9b)$$

$$\underline{n}_i(2) = \underline{N}(1-\underline{g}_i)(\underline{a}_i^2 \underline{d}_i^2 + \underline{c}_i^2 \underline{b}_i^2 + 4\underline{a}_i \underline{c}_i \underline{b}_i \underline{d}_i), \quad (9c)$$

$$\underline{n}_i(1) = \underline{N}(1-\underline{g}_i)(2\underline{a}_i \underline{c}_i \underline{d}_i^2 + 2\underline{c}_i^2 \underline{b}_i \underline{d}_i), \quad (9d)$$

$$\underline{n}_i(0) = \underline{N}(1-\underline{g}_i)(\underline{c}_i^2 \underline{d}_i^2). \quad (9e)$$

At this point, a computer is needed to determine which set of aluminum site occupancy values $\{g_1, g_2, g_3\}$ best matches the experimental peak areas for a particular assignment scheme. An outline of the program is as follows:

- (1) Loop over the allowed $g_1, g_2,$ and g_3 values in increments of 0.01.
- (2) For every triad of g_i values, calculate the number of silicons in each T_i site with k Al neighbors.
- (3) Combine these numbers according to the assignment scheme.
- (4) Scale the simulated intensities to provide the best weighted-least-squares fit to the experimental peak areas.
- (5) Calculate the rms error for each $\{g_1, g_2, g_3\}$ combination, and keep track of the "winners."

Results for the Mt. Cimini/Rocca Monfina leucite spectrum with assignment schemes I-IV are listed in Table 6. Clearly, assignment scheme I generates the best rms fit to the experimental peak areas as well as the best match to the electron microprobe Si/Al values found in Table 1. It should be stressed that in the computer program described above, the Si/Al ratio was free to vary from $\underline{R}=1.0$ to $\underline{R}=99.0$. That the Al distribution providing the best fit to the spectrum also agrees well with the experimental Si/Al ratio lends credence to this model of tetrahedral cation ordering.

In addition, we tried assignment scheme I but without the constraint of aluminum avoidance. (In this case, the denominator for each $P(i,j)$ and $Q(i,j)$ expression equals one.) The rms error in fitting peak areas and the deviation from the correct R value are comparable to or larger than those of any of the aluminum-avoidance schemes, implying that Loewenstein's rule is, as expected, operative in these minerals.

Also in Table 6 are results for the heat-treated and gel-synthesized leucites. In all three samples, an inequality exists in the aluminum occupancy of the three T_i sites, with T_3 the most hospitable to Al cations and T_2 the least so. The extent of this site preference is more pronounced in the natural leucite than in the gel-synthesized sample. For natural leucite, the difference in g_i values before and after heat treatment may possibly be a real effect, but is much more likely an indication of the uncertainties in the analysis: the average deviation for each g_i value is probably on the order of ± 0.03 .

Model 2

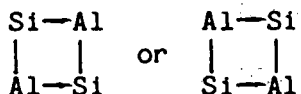
As noted earlier, the previous model incorporates a variable Al occupancy for each T_i site and an aluminum-avoidance effect, but otherwise assumes a random distribution of Al and Si. As a consequence, the relative abundance of various silicon species can be expressed in terms of simple probability relationships. There may exist, however, additional constraints or tendencies that affect the actual Si-Al distribution. An example is Dempsey's rule (Dempsey et al. 1969; Vega 1983), which in generalized form states that for electrostatic reasons, the number of Al-Si-Al linkages should be minimized.

To investigate possible non-random cation distributions and to better fit the experimental peak areas, we have devised a "directed jump" simulational technique, inspired by the method Vega (1983) has used to study adherence to Dempsey's rule in zeolites. Our starting point is a $3 \times 3 \times 3$ array of unit cells with periodic boundary conditions. The 1296 tetrahedral sites (48 in each of the 27 unit cells) constitute a leucite microcosm, one that is meant to be large enough to allow for a wide variety of Si-Al configurations but small enough to be analyzed in a reasonable amount of computer time. In accord with the \underline{R} value of choice, a semi-random pattern of Al cations is scattered among the tetrahedral sites, which otherwise are assumed to contain silicon. Next an initial set of simulated peak areas is generated, based on the relative number of each type of silicon present and the assignment scheme one has selected. The rms error in fitting the experimental peaks is computed and stored as the current "record." A silicon and an aluminum cation are then selected randomly for a possible swap in position on the lattice. For the swap to be allowed, no violations of the aluminum-avoidance rule can occur, and the resulting set of simulated peak areas must be a better fit to the experimental spectrum. If the move is allowed, the rms error record is also updated. The process continues until selected Si-Al swaps fail to break the error record 1000 times in a row. The entire procedure is then repeated several times in an attempt to obtain the best possible fit for a particular value of \underline{R} . Finally, in the outermost loop of the program, the input Si/Al ratio itself is varied over a narrow range about its experimentally determined value, again in the quest for an optimum fit. (We chose the increment in Si/Al values to be 0.05.)

Listed in Table 7 are results for "winning" distributions found for each of the three leucite samples. When two different Si/Al ratios produced comparably small rms error values, both data sets are listed. Two observations can be made. First, the aluminum distributions generated by this directed jump simulation are in remarkably good agreement with those of model 1 for natural leucite, with and without heat treatment. For the gel-synthesized sample, however, a more differentiated Al distribution is generated, a distribution more like (but not identical to) that found for natural leucite. Second, for all three samples, the quality of the fit, as evidenced by the optimized rms error values, is noticeably improved relative to model 1. This improvement suggests that there likely is more to the Si-Al distribution in leucites than T_1 site preferences and aluminum avoidance. The nature of this non-random character is difficult to pinpoint, however, as is discussed below.

Additional Thoughts Regarding the Si-Al Distribution

In trying to better understand the distribution of tetrahedral cations in leucite, it is helpful to idealize the site occupancy data somewhat. Assume that for natural leucite, the Al occupancies are simple fractions, equal within error to the model 1 and model 2 results: $\underline{g}_1=0.375$, $\underline{g}_2=0.125$, $\underline{g}_3=0.5$, and $\underline{R}=2.00$. Now imagine that the final distribution of Al cations is generated in two hypothetical steps. First, assume that all aluminums are in T_1 or T_3 sites: $\underline{g}_1=\underline{g}_3=0.5$, $\underline{g}_2=0.0$. In this configuration, all T_1 or T_3 silicons would have exactly two Al neighbors. In contrast, a T_2 silicon could have anywhere from zero to four Al neighbors, because a choice of occupancies would exist for every T_1 or T_3 four-membered ring:



As the second step in producing an idealized natural leucite distribution, merely assume that a quarter of the aluminums in T_1 sites are interchanged with silicons in T_2 sites in accord with Loewenstein's rule.

But what of randomness in the resulting distribution? Let us focus on the unheated Mt. Cimini/Rocca Monfina spectrum, for which we have run the most model 2 simulations. For every successful fit, the directed jump program lists the relative number of each $T_i(kAl)$ silicon species present, including the site identities T_j of the k Al neighbors. We are wary of interpreting this wealth of information too intensely, since much of the predicted structural detail may be chimeric in light of the uncertainties in the lineshape deconvolution process. Nevertheless, one question that can be investigated is whether the Si-Al configuration in four-membered rings is correlated from one ring to the next. Specifically, let us examine the T_3 rings, almost all of which are composed of two silicate and two aluminate tetrahedra for $g_3=0.48$. The relative configuration of these rings is mirrored in the distribution of T_3 Al neighbors per T_2 silicon. From Eq. 6, the probability of a single Si[T_2]-Al[T_3] bond is given by

$$\underline{p} = \underline{P}(2,3) = \frac{g_3}{1 - g_2} \quad (10)$$

If the pattern of T_3 ring occupancies is random, then the ratio of T_2 silicons with zero, one, or two T_3 Al neighbors is $(1-\underline{p})^2 : 2\underline{p}(1-\underline{p}) : \underline{p}^2$. For $g_2=0.48$, $g_3=0.14$, and $\underline{p}=0.56$, this ratio is 0.20 : 0.49 : 0.31. A non-random T_3 ring pattern would result in an excess or shortage of silicons with one T_3 Al neighbor relative to the number of silicons with zero or two such neighbors. Results from four different model 2

simulations with minimal relative error (less than 0.35%) in fitting the experimental lineshape are as follows: the number of T_2 silicons with one T_3 Al neighbor obtained using model 2 divided by the number expected for a random distribution of ring configurations was found to be 1.23, 1.03, 1.15, and 1.12. That these values are consistently greater than one suggests that some degree of ring-to-ring correlation of T_3 cations may be present in leucite.

A second question that can be examined is whether electrostatically unfavorable Al-Si-Al linkages are minimized in accord with Dempsey's rule. Following Vega (1983), we count the number of such linkages by considering, for a given silicon, the number of ways \underline{n}_D of selecting \underline{k} Al neighbors two at a time: $\underline{n}_D=0,0,1,3,6$ for $\underline{k}=0,1,2,3,4$. For a random distribution of Al and Si subject only to Loewenstein's aluminum-avoidance effect, the average number of Al-Si-Al linkages per silicon is given by

$$\langle \underline{n}_D \rangle = 6 / \underline{R}^2 \quad (11)$$

For unheated natural leucite with $\underline{R}=2.05$, this overall $\langle \underline{n}_D \rangle$ value equals 1.43. However, the preferential siting of aluminum in T_1 and T_3 positions lowers the number of Al-Si-Al linkages by minimizing the concentration of $T_1(4Al)$ silicons. For a random arrangement of tetrahedral cations constrained by Loewenstein's rule and by the Al site occupancy fractions in Table 7 (i.e., a distribution consistent with model 1), the average number of Al-Si-Al linkages per silicon is 1.38. In contrast, from the detailed Si-Al connectivity information generated by the two model 2 simulations that correspond to the \underline{g}_1 values in Table 7, we find 1.38 and 1.37 Al-Si-Al linkages per silicon. That is to say, whatever additional

non-random character is present in the model 2 distributions that best match the experimental spectrum, it does not appreciably affect the number of Al-Si-Al linkages: Dempsey's rule is apparently not a driving force for distributional variation beyond the T_1 site preference effect. It should be noted, however, that relative to comparable model 1 results, the model 2 simulations predict a greater number of silicons with two or four Al neighbors and a lesser number with three Al neighbors.

ANALYSIS OF THE ANALCITE SPECTRUM

Model 1 and model 2 simulations were also run to fit the peak areas listed in Table 2 for analcite. As noted earlier, because of the lack of an intrinsic site shift, each peak in the spectrum corresponds to a particular value of k , the number of Al neighbors. The symmetry is assumed to be tetragonal $I4_1/a$ or very nearly so; as a consequence, sites T_1 and T_3 are equivalent and g_1 should equal g_3 . Our results appear in Table 8. Both models find that two distinctly different Si-Al distributions give rise to minimal rms error values. In what we will call distribution A, aluminum cations are concentrated in the T_2 sites: $g_2=0.76-0.78$. In distribution B, almost all Al cations occupy $T_1=T_3$ sites: $g_2=0.02-0.04$. (In contrast, constraining the three g_i values to be equal maximizes the rms error.)

It is impossible to choose between these two distributional models on the basis of our analcite NMR data alone. Had the potassium-exchanged analcite sample yielded a measurable spectrum, the ambiguity could be resolved using the extra information provided by intrinsic T_1 chemical shifts. Alternatively, Mazzi and Galli (1978) have correlated aluminum

occupancy with unit-cell dimensions: g_2 is proportional to the unit-cell edge along the c -axis; $g_1 = g_3$ is proportional to the unit-cell edge along the a -axis. A careful single-crystal x-ray determination of the unit-cell dimensions in our analcite sample should therefore allow us to select the correct distribution.

This measurement has not yet been made. We should note, however, that Mazzi and Galli proposed no value of g_2 higher than 0.50 for the seven analcite samples they analyzed. In addition, these authors developed several models for ordering in analcite that minimize electrostatic charge on framework oxygens by correlating g_i values with the occupancy of sodium ions in adjacent S sites. Their simplest model (Galli et al. 1978), that the Al fraction in a T_i site is half the adjacent Na occupancy, yields a maximum g_2 value of 0.5. A more detailed analysis (Mazzi and Galli 1978) relates the Na occupancy to $0.75(g_2) + 5/12$, for which the maximum g_2 value is 7/9 or approximately 0.778. When the effect of water molecules is included to better fit their experimental data, the maximum g_2 value becomes 0.6. Only the second of these models is compatible with distribution A.

CONCLUSIONS

As has been demonstrated previously in the study of zeolites, ^{29}Si magic-angle-spinning NMR spectroscopy can provide detailed information on silicon-aluminum ordering in minerals. On the basis of our data and the two distributional models we have investigated, we can conclude the following:

(1) Contrary to interpretations based on single-crystal x-ray work, the Si-Al distribution in leucite is not purely random: aluminum occupancy fractions for the three T_1 sites are distinctly different. Distribution model 1 (random arrangement of Al cations subject to T_1 site preferences and Loewenstein's aluminum-avoidance effect) yields $g_1=0.41$, $g_2=0.09$, and $g_3=0.50$ for a Mt. Cimini/Rocca Monfina sample. Model 2 (directed "Loewensteinian" jumping of Al cations on a lattice of tetrahedral sites to minimize the error in fitting experimental data) generates a similar set of values: $g_1=0.37$, $g_2=0.14$, and $g_3=0.48$.

(2) Aluminum site preferences are less pronounced in the gel-synthesized leucite sample, as one might expect for crystals that grew rapidly from a presumably disordered gel. Model 1 yields $g_1=0.34$, $g_2=0.26$, and $g_3=0.38$; model 2 yields $g_1=0.36$, $g_2=0.18$, and $g_3=0.42$.

(3) Heat treatment of the Mt. Cimini leucite sample at 1673K for a week, which modifies its tetragonal-cubic phase transition, has minimal apparent effect on the short-range Si-Al distribution.

(4) The additional non-random character inherent in the model 2 simulations is not readily identifiable. For natural leucite, there may exist some correlation in the configuration of adjacent T_3 rings. However, beyond the differentiation in g_i values, there is no apparent manifestation of Dempsey's Al-Si-Al linkage minimization rule.

(5) In fitting the experimental peak areas of analcite, both model 1 and model 2 simulations generate two distinctly different distributions A and B, the former with aluminum predominantly in T_2 sites ($g_1=g_3=0.09$, $g_2=0.78$), the latter with only a scattering of T_2 Al cations ($g_1=g_3=0.46$, $g_2=0.04$). A choice between distributions A and B could likely be made based on the spectrum of a K-exchanged sample or the unit-cell dimensions.

The detailed information on silicon-aluminum ordering in tectosilicates that can be obtained with ^{29}Si (and ^{27}Al) MAS NMR has been of great use in the design of zeolite catalysts for the chemical industry. Petrologic applications remain largely for future work but are potentially wide: cation distributions often reflect the geologically important variables of time, temperature, and composition. The ordering state of feldspar, as determined by x-ray diffraction and optical means, is an often-used clue to the temperature of ordering and to growth kinetics. Similar constraints on geochemical processes may be obtainable from studies of natural zeolites and feldspathoids. As a small start, we have shown here that leucite phenocrysts from very similar lavas of the Roman province are structurally nearly identical, but that material from the groundmass of a wyomingite lava is qualitatively different.

In short, now that the analytical tools have been developed, opportunities for future work include a more thorough investigation of Si-Al ordering in a variety of leucite minerals of different origin and thermal history. Ion exchange (with the inclusion of paramagnetic impurities to facilitate relaxation) will allow the direct comparison of distributional results from leucite-like and analcite-like spectra: one with and the other without intrinsic T_{i} site chemical shifts. Finally, the calibration of ordering with experimentally determined temperature and time of synthesis may provide new quantitative data on the origin of these types of minerals in nature.

ACKNOWLEDGMENTS

We would like to thank R. Lange in particular for supplying the gel-synthesized leucite sample and B. Mysen for sending us a copy of the Raman lineshape-fitting program that we modified for NMR analysis. This work was supported by the Director, Office of Basic Energy Sciences, Division of Engineering, Mathematics, and Geosciences of the U.S. Department of Energy under contract DEAC03-76SF00098; and by the National Science Foundation, grant number EAR-8507925.

REFERENCES

- Abragam A (1961) The Principles of Nuclear Magnetism. Oxford University Press, London
- Andrew ER (1981) Magic angle spinning in solid state n.m.r. spectroscopy. Phil Trans Roy Soc London A:505-520
- Barron PF, Frost RL, Skjemstad JO (1983) ^{29}Si spin-lattice relaxation in aluminosilicates. J Chem Soc Chem Commun : 581-583
- Beger RM (1969) The crystal structure and chemical composition of pollucite. Z Kristallogr 129:280-302
- Carmichael ISE (1967) The mineralogy and petrology of the volcanic rocks from the Leucite Hills, Wyoming. Contrib Mineral Petrol 15:24-66
- Dempsey E, Kuhl GH, Olsen DH (1969) Variation of the lattice parameter with aluminum content in synthetic sodium faujasites. Evidence for ordering of the framework cations. J Chem Phys 73:387-390
- Engelhardt G, Radeglia R (1984) A semi-empirical quantum-chemical rationalization of the correlation between SiOSi angles and ^{29}Si NMR chemical shifts of silica polymorphs and framework aluminosilicates (zeolites). Chem Phys Lett 108:271-274

- Ferraris G, Jones DW, Yerkess J (1972) A neutron-diffraction study of the crystal structure of analcime, $\text{NaAlSi}_2\text{O}_6 \cdot \text{H}_2\text{O}$. *Z Kristallogr* 135:240-252
- Fyfe CA, Thomas JM, Klinowski J, Gobbi GC (1983) Magic-angle-spinning NMR (MAS-NMR) spectroscopy and the structure of zeolites. *Angew Chem Int Ed Engl* 22:259-275
- Galli E, Gottardi G, Mazzi F (1978) The natural and synthetic phases with the leucite framework. *Miner Petrogr Acta* 22:185-193
- Grimmer AR (1985) Correlation between individual Si-O bond lengths and the principal values of the ^{29}Si chemical shift tensor in solid silicates. *Chem Phys Lett* 119:416-420
- Grimmer AR, Radeaglia R (1984) Correlation between the isotropic ^{29}Si chemical shifts and the mean silicon-oxygen bond lengths in silicates. *Chem Phys Lett* 106:262-265
- Higgins JB, Woessner DE (1982) ^{29}Si , ^{27}Al , and ^{23}Na spectra of framework silicates. *Trans Am Geophys Union (EOS)* 63:1139
- Jarman RH, Jacobson AJ, Melchior MT (1984) Interpretation of the silicon-29 nuclear magnetic resonance spectra of zeolites: synthetic mazzite. *J Phys Chem* 88:5748-5752

- Klinowski J, Anderson MW (1986) A high-resolution solid-state nuclear magnetic resonance study of the ordering of silicon and aluminium in synthetic mazzite (zeolite omega). *J Chem Soc Faraday Trans 1* 82:569-584
- Klinowski J, Ramdas S, Thomas JM (1982) A re-examination of Si,Al ordering in zeolites NaX and NaY. *J Chem Soc Faraday Trans 2* 78:1025-1050
- Lange R, Carmichael ISE, Stebbins JF (1986) Phase transitions in leucite (KAlSi_2O_6), orthorhombic KAlSiO_4 , and their iron analogs (KFeSi_2O_6 , KFeSiO_4). *Am Mineral* 71:937-945
- Lippmaa E, Magi M, Samoson A, Engelhardt G, Grimmer AR (1980) Structural studies of silicates by solid-state high-resolution ^{29}Si NMR. *J Am Chem Soc* 102:4889-4893
- Lippmaa E, Magi M, Samoson A, Tarmak M, Engelhardt G (1981) Investigation of the structure of zeolites by solid-state high-resolution ^{29}Si NMR spectroscopy. *J Am Chem Soc* 103:4992-4996
- Loewenstein W (1954) The distribution of aluminum in the tetrahedra of silicates and aluminates. *Am Mineral* 39:92-96
- Mazzi F, Galli E (1978) Is each analcime different? *Am Mineral* 63:448-460
- Mazzi F, Galli E, Gottardi G (1976) The crystal structure of tetragonal leucite. *Am Mineral* 61:108-115

- Merlino S (1984) Feldspathoids: their average and real structure. In:
Brown WL (ed) Feldspars and Feldspathoids (NATO Advanced Study
Institute). Reidel Publishing Co, New York, pp 435-470
- Murdoch JB, Stebbins JF, Carmichael ISE (1984) Silicon-29 MAS nuclear
magnetic resonance study of the structure of feldspathoid minerals.
Geol Soc Am Abst w Prog 16, 6:604
- Murdoch JB, Stebbins JF, Carmichael ISE (1985) High-resolution ^{29}Si NMR
study of silicate and aluminosilicate glasses: the effect of network-
modifying cations. Am Mineral 70:332-343
- Peacor DR (1968) A high temperature single crystal diffractometer study of
leucite, $(\text{K},\text{Na})\text{AlSi}_2\text{O}_6$. Z Kristallogr 127:213-224
- Putnis A, Fyfe CA, Gobbi GC (1985) Al,Si ordering in cordierite using
"magic angle spinning" NMR. I. Si^{29} spectra of synthetic cordierites.
Phys Chem Minerals 12:211-216
- Putnis A, Angel RJ (1985) Al,Si ordering in cordierite using "magic angle
spinning" NMR. II. Models of Al,Si order from NMR data. Phys Chem
Minerals 12:217-222
- Radeglia R, Engelhardt G (1985) Correlation of Si-O-T (T = Si or Al) angles
and ^{29}Si NMR chemical shifts in silicates and aluminosilicates.
Interpretation by semi-empirical quantum-chemical considerations.
Chem Phys Lett 114:28-30

Ramdas S, Klinowski J (1984) A simple correlation between isotropic ^{29}Si -NMR chemical shifts and T-O-T angles in zeolite frameworks. Nature 308:521-523

Smith JV (1982) Geometrical and Structural Crystallography. Wiley, New York

Smith JV, Blackwell CS (1983) Nuclear magnetic resonance of silica polymorphs. Nature 303:223-225

Smith KA, Kirkpatrick RJ, Oldfield E, Henderson DM (1983) High-resolution silicon-29 nuclear magnetic resonance spectroscopic study of rock-forming silicates. Am Mineral 68:1206-1215

Stebbins JF, Murdoch JB, Carmichael ISE, Pines A (1986) Defects and short-range order in nepheline group minerals: a silicon-29 nuclear magnetic resonance study. Phys Chem Minerals, in press

Taylor WH (1930) The structure of analcite ($\text{NaAlSi}_2\text{O}_6 \cdot \text{H}_2\text{O}$). Z Kristallogr 74:1-19

Thomas JM, Klinowski J, Ramdas S, Hunter BK, Tennakoon DTB (1983) The evaluation of non-equivalent tetrahedral sites from ^{29}Si NMR chemical shifts in zeolites and related aluminosilicates. Chem Phys Lett 102:158-162

Vega AJ (1983) A statistical approach to the interpretation of silicon-29 NMR of zeolites. In: Stucky GD, Dwyer FG (eds) Intrazeolite Chemistry. American Chemical Society, Washington, D.C., pp 217-230

Waldbaum DR, Robie RA (1971) Calorimetric investigation of Na-K mixing and polymorphism in the alkali feldspars. Z Kristallogr 184:381-420

TABLE 1

Silicon-to-aluminum ratios from
chemical analysis of leucite and analcite samples^{1,2}.

	Heat-treated		Rocca		Gel-	
	Mt. Cimini	Mt. Cimini	Monfina	Wyomingite	synthesized	Analcite
	leucite	leucite	leucite	leucite	leucite ³	
Si/Al ratio	2.05	2.02	2.06	2.35	2.09	2.13

¹Leucite analyses from Lange et al. (1986).

²Electron microprobe data, except where noted.

³Wet chemical data.

TABLE 2

Deconvolution of the analcite spectrum into Gaussian components.

Peak	Chemical shift (ppm)	FWHM ¹ (ppm)	Relative area (%)	Number of Al neighbors
1	-91.6	3.5	14.8 ± 0.3	3
2	-96.8	3.1	59.7 ± 0.3	2
3	-102.0	3.3	23.4 ± 0.3	1
4	-106.9	3.4	2.0 ± 0.3	0

¹Full width at half-maximum of the Gaussian component.

TABLE 3

Deconvolution of the leucite spectra into Gaussian components.

Sample	Peak	Chemical shift (ppm)	FWHM (ppm)	Relative area (%)
Natural				
leucite	1	-78.7	5.2	3.6 ± 0.2
	2	-81.4	2.3	5.1 ± 0.2
	3	-85.3	3.4	17.2 ± 0.3
	4	-88.4	2.8	8.7 ± 0.4
	5	-92.2	4.6	28.2 ± 0.5
	6	-97.6	4.1	21.9 ± 0.3
	7	-102.3	4.2	10.0 ± 0.5
	8	-106.7	6.7	5.2 ± 0.4
Heat-treated				
leucite	1	-78.4	4.4	2.7 ± 0.1
	2	-81.3	2.3	5.4 ± 0.1
	3	-85.2	3.3	16.0 ± 0.3
	4	-88.4	3.0	10.8 ± 0.5
	5	-92.1	4.3	25.1 ± 0.5
	6	-97.5	4.4	23.2 ± 0.3
	7	-102.5	4.0	10.7 ± 0.3
	8	-107.2	6.7	6.0 ± 0.3
Gel-synthesized				
leucite	1	-77.3	3.3	2.6 ± 0.1
	2	-81.3	2.9	8.0 ± 0.1
	3	-85.0	2.7	10.3 ± 0.5
	4	-88.1	4.1	17.1 ± 1.0
	5	-92.4	3.9	22.2 ± 0.6
	6	-97.5	4.7	25.3 ± 0.4
	7	-102.7	3.8	10.0 ± 0.3
	8	-107.2	5.0	4.5 ± 0.3

TABLE 4

Estimated chemical shifts for T_i (kAl) silicon species in leucite¹.

	T_1 sites	T_2 sites	T_3 sites
Average Si-O-T angle ²	145.9°	138.9°	130.4°
δ_{Si} for			
0Al	-109.0	-103.8	-96.3
1Al	-103.5	-98.3	-90.7
2Al	-98.1	-92.9	-85.2
3Al	-92.7	-87.4	-79.6
4Al	-87.3	-81.9	-74.1

¹Calculated using Eq. 1, a relationship derived by Ramdas and Klinowski (1984).

²From bond angles obtained by Mazzi et al. (1976).

TABLE 5

Leucite peak assignment schemes.

Peak	SCHEME I	SCHEME II
1		$T_3(4A1)$
2		$T_3(3A1)$
3	$T_2(4A1) + T_3(2A1)$	$T_3(2A1)$
4	$T_1(4A1) + T_2(3A1) + T_3(1A1)$	$T_1(4A1) + T_2(4A1) + T_3(1A1)$
5	$T_1(3A1) + T_2(2A1) + T_3(0A1)$	$T_1(3A1) + T_2(3A1) + T_3(0A1)$
6	$T_1(2A1) + T_2(1A1)$	$T_1(2A1) + T_2(2A1)$
7	$T_1(1A1) + T_2(0A1)$	$T_1(1A1) + T_2(1A1)$
8	$T_1(0A1)$	$T_1(0A1) + T_2(0A1)$

Peak	SCHEME III	SCHEME IV
1		$T_3(3A1)$
2		$T_3(2A1)$
3	$T_2(4A1) + T_3(1A1)$	$T_3(1A1)$
4	$T_1(4A1) + T_2(3A1) + T_3(0A1)$	$T_1(4A1) + T_2(4A1) + T_3(0A1)$
5	$T_1(3A1) + T_2(2A1)$	$T_1(3A1) + T_2(3A1)$
6	$T_1(2A1) + T_2(1A1)$	$T_1(2A1) + T_2(2A1)$
7	$T_1(1A1) + T_2(0A1)$	$T_1(1A1) + T_2(1A1)$
8	$T_1(0A1)$	$T_1(0A1) + T_2(0A1)$

TABLE 6

Model 1 simulation values for aluminum T_i site occupancies in leucite.

Sample	Assignment scheme	Al avoidance	\underline{g}_1	\underline{g}_2	\underline{g}_3	Si/Al ratio	Relative rms error (%)
Natural							
leucite	I	yes	0.41	0.09	0.50	2.00	18.9
	II	yes	0.50	0.17	0.42	1.75	20.6
	III	yes	0.44	0.15	0.27	2.49	23.7
	IV	yes	0.50	0.18	0.25	2.23	23.9
	I	no	0.41	0.48	0.53	1.11	23.2
Heat-treated							
leucite	I	yes	0.39	0.11	0.46	2.13	13.8
Gel-synthesized							
leucite	I	yes	0.34	0.26	0.38	2.06	8.7

TABLE 7

Model 2 simulation values for aluminum $T_{\underline{i}}$ site occupancies in leucite.

Sample	Si/Al ratio	\underline{g}_1	\underline{g}_2	\underline{g}_3	Relative rms error (%)
Natural leucite	2.05	0.37	0.14	0.48	0.32
Heat-treated leucite	2.10	0.36	0.13	0.48	1.11
	2.15	0.35	0.14	0.46	0.23
Gel- synthesized leucite	2.10	0.36	0.17	0.44	0.46
	2.15	0.36	0.19	0.41	0.28

TABLE 8

Model 1 and model 2 simulation values
for the aluminum T_1 site occupancies in analcite.

Model	Distribution	Si/Al ratio	ξ_1	ξ_2	ξ_3	Relative rms error (%)
1	A	2.13	0.10	0.76	0.10	2.5
1	B	2.13	0.47	0.02	0.47	5.6
2	A	2.15	0.08	0.79	0.08	1.7
2	B	2.15	0.46	0.04	0.45	3.0

FIGURE CAPTIONS

- Fig. 1 An idealized unit cell for leucite group minerals that illustrates the connectivity of the 48 tetrahedral sites. Circles represent tetrahedral cations (Si or Al) and oxygens are omitted. The view is approximately along the c -axis, and the three types of crystallographically distinct T_1 sites in low-temperature leucite (space group $I4_1/a$) are displayed.
- Fig. 2 The ^{29}Si MAS NMR spectrum of analcite (1259 acquisitions with a recycle time -- the interval between successive rf pulses -- of 40 sec). The chemical shift δ is given in ppm relative to a tetramethylsilane standard. In this and subsequent spectra, the thick solid line is the experimental lineshape, the dotted line is the overall simulated spectrum, and the thin solid lines delineate the individual Gaussian components that contribute to the simulation. The small spinning sidebands are not shown; they lie beyond the range of this plot.
- Fig. 3 The ^{29}Si MAS NMR spectrum of dehydrated analcite (662 acquisitions, 120 sec recycle time).
- Fig. 4 A weighted sum of ^{29}Si MAS NMR spectra for the Mt. Cimini and Rocca Monfina leucite samples (Mt. Cimini leucite: 1077 acquisitions, 40 sec recycle time + 2000 acquisitions, 5 sec recycle time; Rocca Monfina leucite: 2647 acquisitions, 15 sec recycle time).

Fig. 5 The ^{29}Si MAS NMR spectrum of the heat-treated Mt. Cimini leucite sample (1501 acquisitions, 20 sec recycle time + 4292 acquisitions, 15 sec recycle time + 2500 acquisitions, 4 sec recycle time).

Fig. 6 The ^{29}Si MAS NMR spectrum of gel-synthesized leucite (1716 acquisitions, 40 sec recycle time).

Fig. 7 The ^{29}Si MAS NMR spectrum of wyomingite groundmass leucite (316 acquisitions, 30 sec recycle time + 758 acquisitions, 60 sec recycle time).

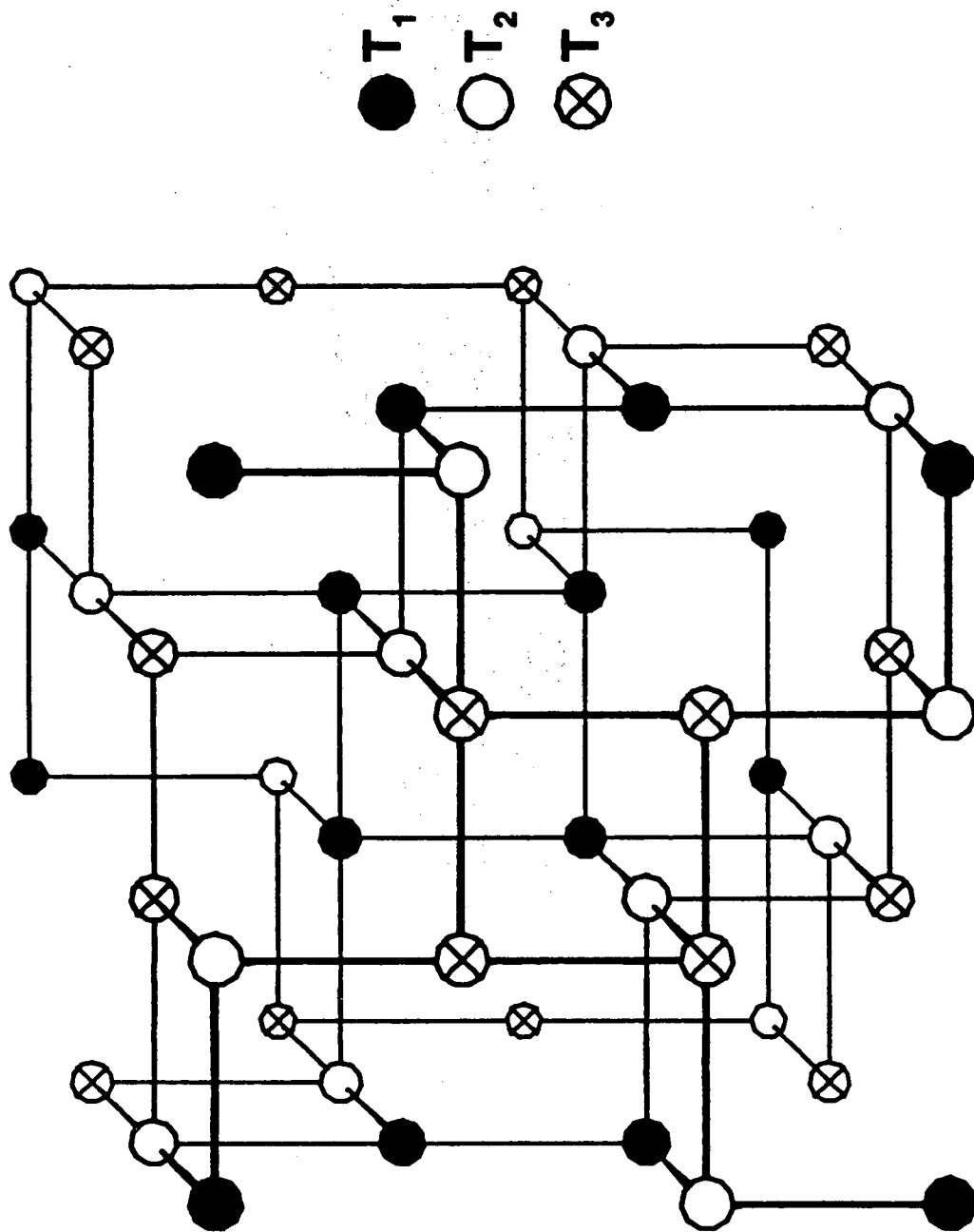


Figure 1

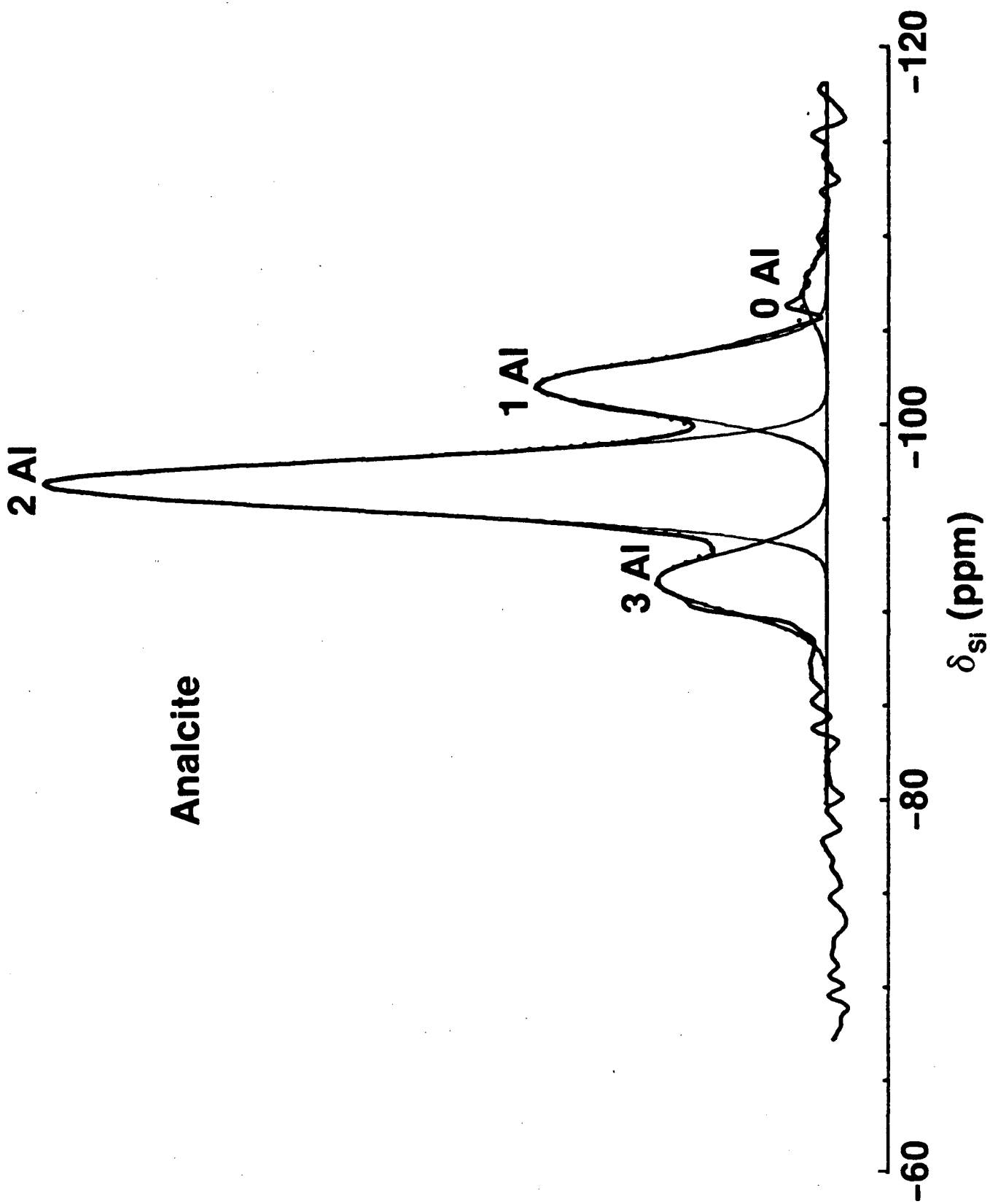


Figure 2

**Dehydrated
Analcite**

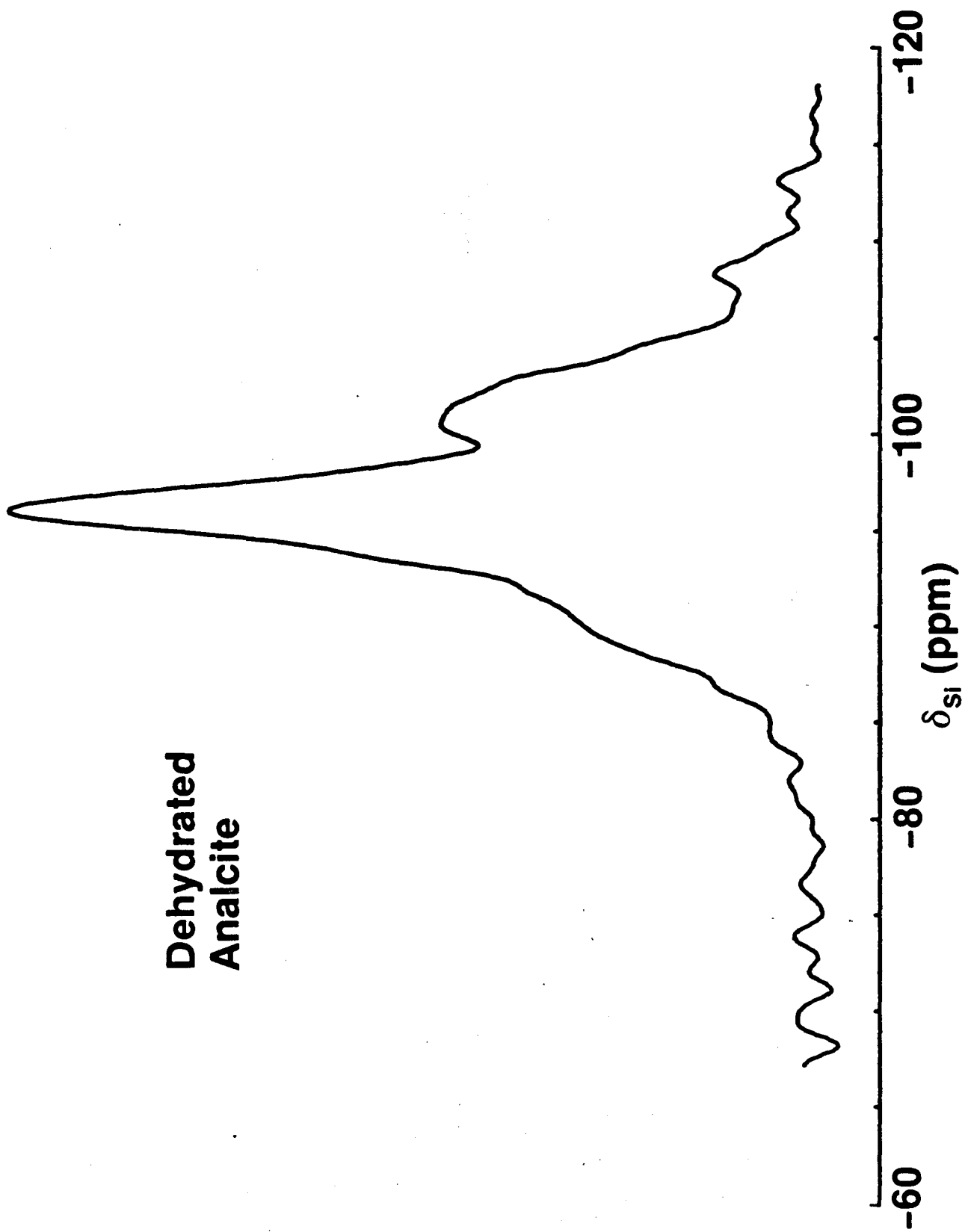
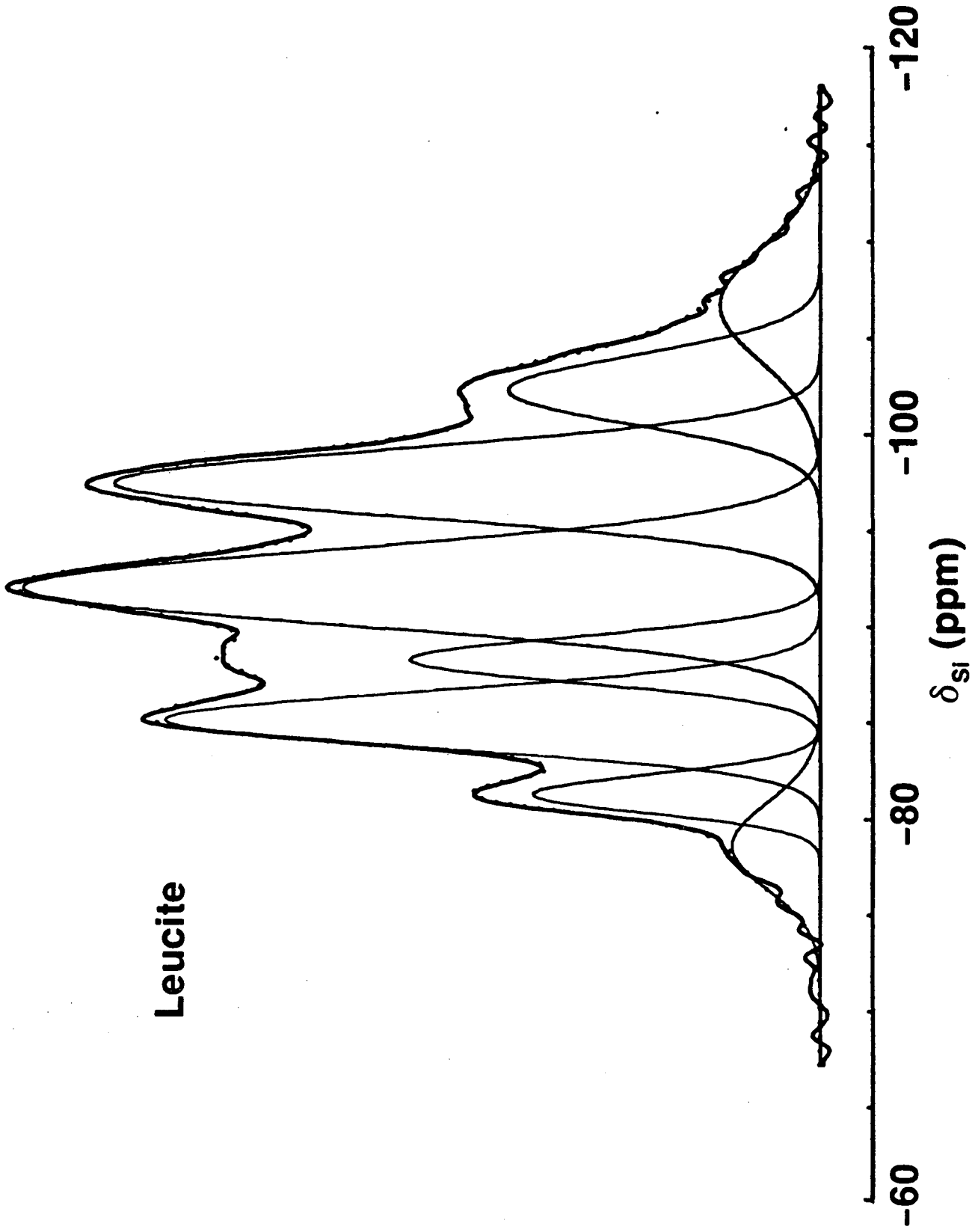


Figure 3



Leucite

Figure 4

**Heat-Treated
Leucite**

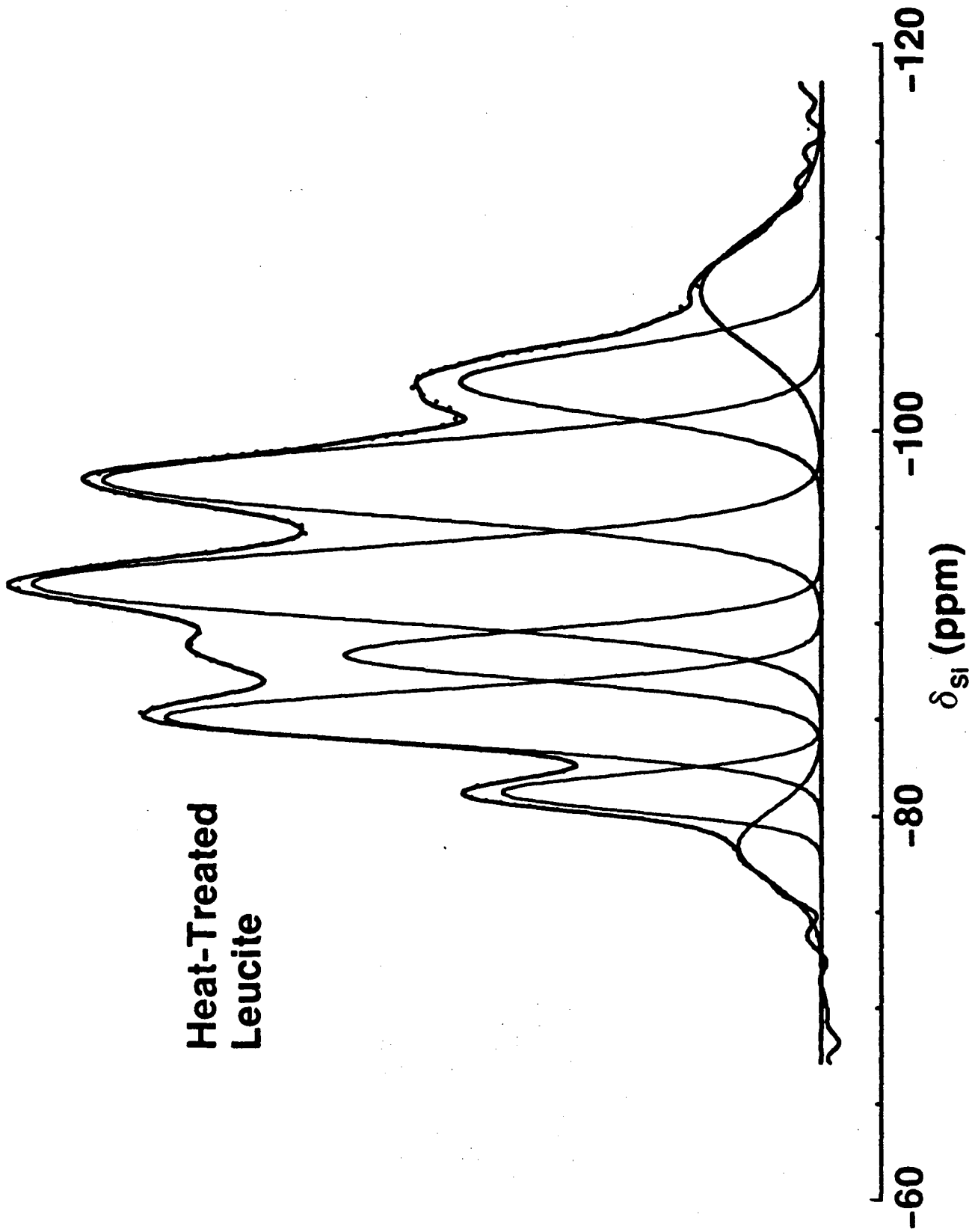


Figure 5

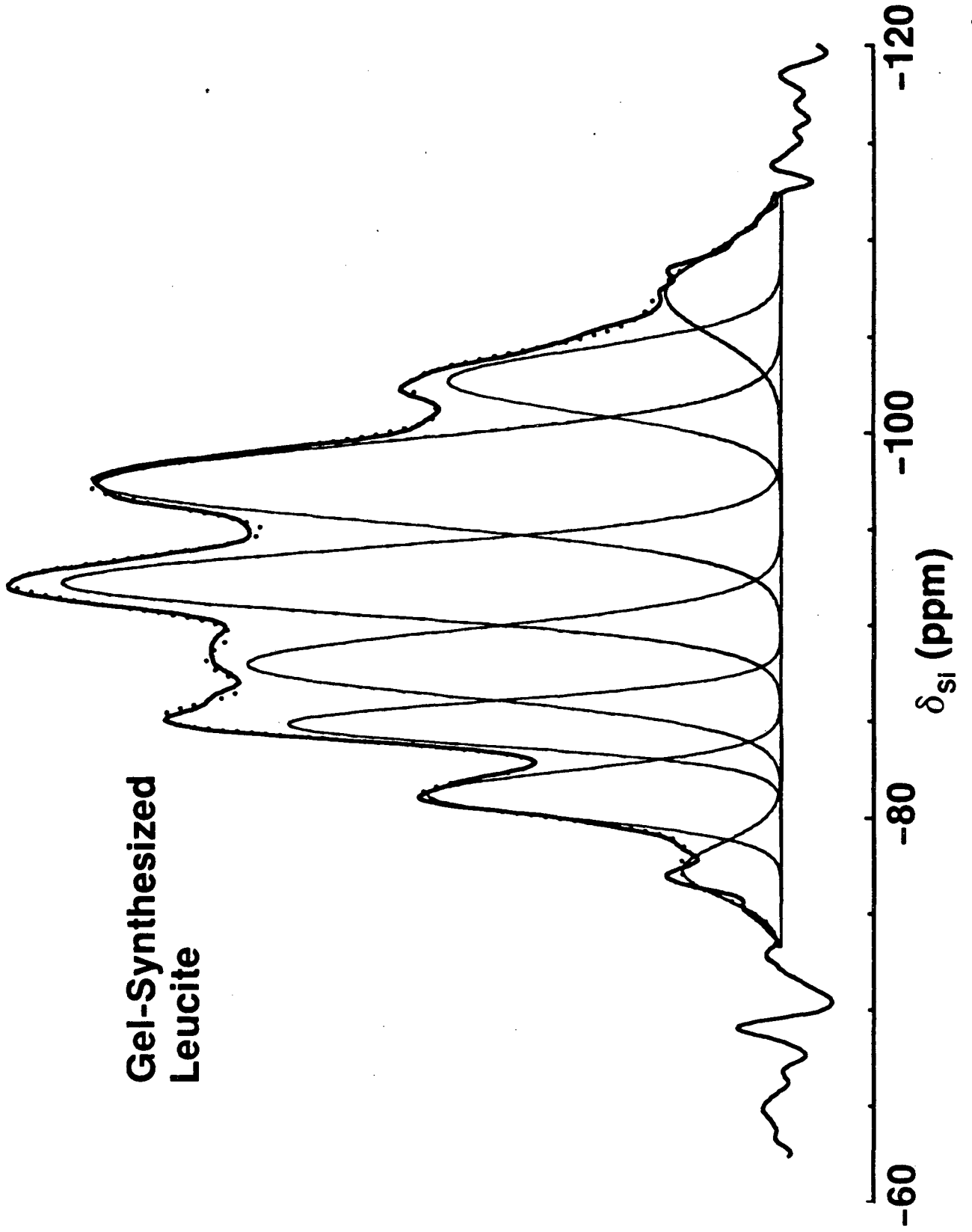
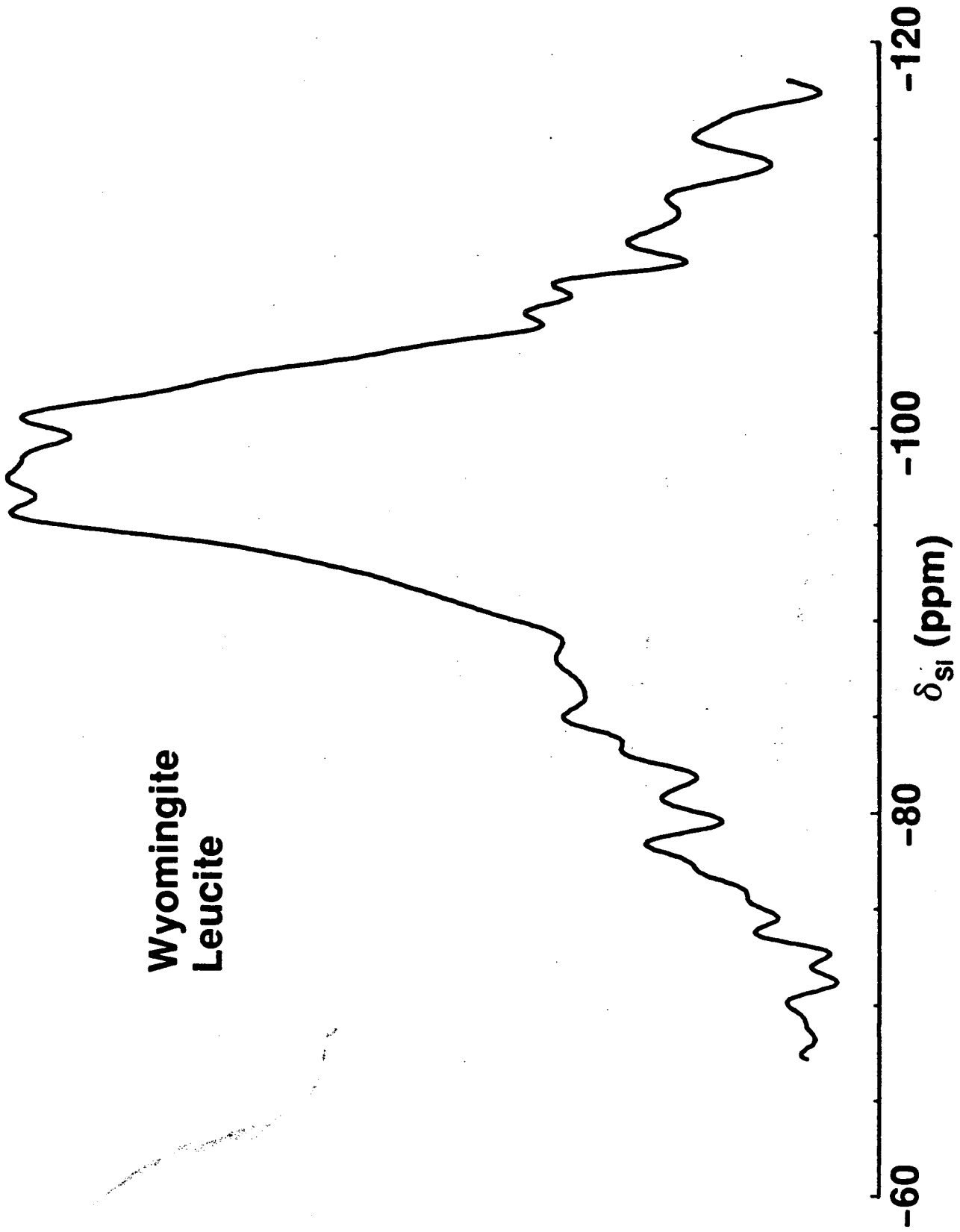


Figure 6



**Wyomingite
Leucite**

Figure 7

This report was done with support from the Department of Energy. Any conclusions or opinions expressed in this report represent solely those of the author(s) and not necessarily those of The Regents of the University of California, the Lawrence Berkeley Laboratory or the Department of Energy.

Reference to a company or product name does not imply approval or recommendation of the product by the University of California or the U.S. Department of Energy to the exclusion of others that may be suitable.

*LAWRENCE BERKELEY LABORATORY
TECHNICAL INFORMATION DEPARTMENT
UNIVERSITY OF CALIFORNIA
BERKELEY, CALIFORNIA 94720*